

NATIONAL AIR INTELLIGENCE CENTER



EFFECT OF ATMOSPHERIC TURBULENCE ON LASER
BEAM PROPAGATION

by

Guo Zhenhua, Xu Desheng, et al.

DTIC QUALITY INSPECTED 2



Approved for public release:
distribution unlimited

19960408 198

HUMAN TRANSLATION

NAIC-ID(RS)T-0697-95 14 March 1996

MICROFICHE NR: 96000235

EFFECT OF ATMOSPHERIC TURBULENCE ON LASER
BEAM PROPAGATION

By: Guo Zhenhua, Xu Desheng, et al.

English pages: 16

Source: Laser Technology, Vol. 16, Nr. 2, 1992; pp. 65-72

Country of origin: China
Translated by: Leo Kanner Associates
F33657-88-D-2188

Requester: NAIC/TATD/Bruce Armstrong
Approved for public release: distribution unlimited.

THIS TRANSLATION IS A RENDITION OF THE ORIGINAL FOREIGN TEXT WITHOUT ANY ANALYTICAL OR EDITORIAL COMMENT STATEMENTS OR THEORIES ADVOCATED OR IMPLIED ARE THOSE OF THE SOURCE AND DO NOT NECESSARILY REFLECT THE POSITION OR OPINION OF THE NATIONAL AIR INTELLIGENCE CENTER.

PREPARED BY:

TRANSLATION SERVICES
NATIONAL AIR INTELLIGENCE CENTER
WPAFB, OHIO

GRAPHICS DISCLAIMER

All figures, graphics, tables, equations, etc. merged into this translation were extracted from the best quality copy available.

EFFECT OF ATMOSPHERIC TURBULENCE ON LASER
BEAM PROPAGATION

Guo Zhenhua, Xu Desheng, Wang Shipeng,
and Li Zaiguang

National Laboratory of Laser Technology,
Huazhong University of Science and Technology,
Wuhan

[ABSTRACT: In this paper, the effect of atmospheric turbulence on laser beam propagation between tops of the high-building and the hill behind our university campus at the distance of 1500m is discussed. The typical range of measurable C_n values, curvature of the laser beam propagation and the focal spots diameter of the laser beam are given, which are agreement with the theory analysis.

I. Introduction

Applications of laser communications, ranging, guidance, positioning, navigation, reconnaissance, and laser weapons are related to laser transmission in the atmosphere. Various interferences in the atmosphere are related to laser applications, especially the effect of atmospheric turbulence. Some research reports [1,2] were published on the effect of atmospheric turbulence on laser beam transmission. These reports have raised theories such as Kolmogorov's classical theory,

inertial subdomain model, modern theory in the graphic solution method, Markov's approximation, LMSP method, and the saturation zone-induction theory based on resonance concepts.

Because of the unique properties of laser beams, such as high brightness, a laser beam is relatively sensitive with respect to the microstructure of atmospheric turbulence. To link the microscopic structure and its statistical properties, a structure tensor D_i (r -arrow) in the entire turbulence cluster serves to describe the statistical properties. With the turbulence air cluster, the mean-square value of the difference of the moving velocity between two different points is

$$D_{ij}(\vec{r}) = \langle [v_i(\vec{r}_1 + \vec{r}) - v_i(\vec{r}_1)] [v_j(\vec{r}_1 + \vec{r}) - v_j(\vec{r}_1)] \rangle \quad (1)$$

In the equation, v_i and v_j are different velocity components; the angle brackets indicate the overall average; r -arrow is the vector of the line connecting two points. In the locally-homogeneous atmospheric turbulence, Eq. (1) can be simplified as follows:

$$D_{ij}(\vec{r}) = [D_{rr}(r) - D_{tt}(r)] n_i n_j + D_{tt}(r) \delta_{ij} \quad (2)$$

In the equation $\delta_{ij} = \begin{cases} 1 & \text{when } i \text{ is equal to } j \\ 0 & \text{when } i \text{ not equal to } j \end{cases}$

n is the unit vector in the r -arrow direction.

D_{rr} is the structure constant of the wind velocity component parallel to the r -arrow direction; D_{tt} is the structure constant of the wind-velocity component to the r -arrow direction. With respect to incompressible turbulence with free boundaries, $[D_{tt} = \frac{1}{2r} \frac{d}{dr} (r^2 D_{rr})]$. Therefore, the statistical properties of turbulence can be described with a single structure constant D_{rr} , that is,

$$D_{rr} = \langle [v_r(\vec{r}_1 + \vec{r}) - v_r(\vec{r}_1)]^2 \rangle \quad (3)$$

and obeying Kolmogorov's 2/3-squared law, we have

$$D_{rr} = C_v^2 r^{-2/3} \quad (4)$$

In the equation, C_v is the structure function of velocity. Fluctuations of the moving velocity of atmospheric turbulence is closely related to fluctuations in temperature T and induces random variations in refractivity n . After neglecting the humidity effect, about 0.5% to 1%, near the sea-surface level, the conventionally expressed formula is

$$n = 1 + 77.6 (1 + 7.52 \times 10^{-3} \lambda^{-2}) (P/T) 10^{-6} \quad (5)$$

In the equation, λ is the wavelength of light; P is atmospheric pressure. Thus, we can deduce that the refractivity structure function $D_n(r)$ also obeys the 2/3-squared law:

$$D_n(r) = C_n^2 r^{-2/3} \quad (6)$$

with respect to visible light with $\lambda = 6.33 \mu\text{m}$, there is approximately

$$C_n = \{ 79 \times 10^{-6} P/T^2 \} C_T \quad (7)$$

The absolute temperature value is used for atmospheric temperature T , the millibar value for P , C_n and C_T indicate, respectively, the refractivity structure constant and the temperature structure constant. Therefore, by using a temperature pulsation instrument to measure C_T , the statistical properties of turbulence can be given. The unit of C_n is $\text{m}^{-1/3}$; its magnitude indicates turbulence intensity, generally between 8×10^{-9} to $5 \times 10^{-7} \text{m}^{-1/3}$ [3].

In the atmospheric layer, due to atmospheric pressure and temperature varying with height, there is a gradient distribution in the direction vertical to the ground surface for light refractivity n . This phenomenon induces a curved optical path for the laser beam in horizontal transmission. At a distance L , the magnitude h of the deviation from the original position of light spots on the receiving screen should be

$$h = \frac{1}{2}CL^2 \quad (8)$$

In the equation, C is the curvature of the light path. Near sea level and T=293K, we can obtain an approximate expression of the curvature as

$$C = 32.6 + 0.93 \frac{dT}{dh} \quad (9)$$

In the equation, the units of C is $\mu\text{rad}/\text{km}$.

In a far-field receiving screen, the authors observed random fluctuations in light intensity, mainly the scintillation due to atmospheric turbulence. The statistical properties are indicated by the mean-square value of the logarithmic difference of light intensity R. For turbulence with homogeneous intensity, in the far-field region, we have

$$\sigma^2 = \langle (\ln I - \ln I_0)^2 \rangle = B(2\pi/\lambda)^{7/6} L^{11/6} C_n^2 \quad (10)$$

The corresponding plane wave $B=1.23$; and the corresponding spherical-surface wave $B=0.49$.

The random variation n due to turbulence leads directly to light beam drift, so that the light spots on the receiving screen rapidly jump around the central position. Generally, the light beam drift angle is expressed by its mean-square value:

$$\sigma_a^2 = 1.75 C_n^2 L \omega_0^{-1/3} \quad (11)$$

In the equation, ω_0 is the exit pupil of the light beam alignment system.

Atmospheric turbulence scatters the light beam. This is very important to practical applications since the light beam forms an expanded angle Θ upon arriving at the target. In particular, when high-power density is required on the target surface, the expanding angle will enlarge the light-spot dimensions. Generally the following equation is used to calculate the value of Θ .

$$\theta = 4.03 C_n^{6/5} \lambda^{-1/5} L^{3/5} \quad (12)$$

Experimental Observations and Study

The experimental observations were repeatedly carried out in three approaches in three areas, in two periods, from April to June, 1988, and from May to July, 1989. The instruments used were mainly the model HN4-1 150mm He-Ne laser device with a TEM_{00} mode output of 4mW and a divergence angle of 1.4mrad; a model 150A He-Ne laser device with a TEM_{00} mode output power of 60mW, adjustable, and a divergence angle of 0.7mrad; a model MK IV laser beam profile instrument; a model GJZ-1 adjustable focal parallel light tube; and a light instrument mount 2.5m in length (focal length 52.25mm; $f_2=99.19$ mm; entrance pupil $D_1=18$ mm; exit pupil $D_2=110$ mm); a thermometer (0°C to 100°C); receiving screen (precision of X-Y coordinates at 0.5cm, and area approximately 1.0m^2); model W16A intercom; loudspeaker, telephone, and audio amplifier, among other equipment. Fig. 1 shows the layout of the observation equipment. The dashed line indicates the observations made in 1989 with a laser device placed on the ground surface; multiply-reflecting mirrors were used to transmit the light to the top of a building and then to transmit it directly with the purpose of simultaneous measurement on the effect of vibrations of the building foundations.

The light beam quality of the He-Ne laser device is a very good gaussian distribution (TEM_{00} mode) (Fig. 2), as measured with the laser beam profile instrument. The light beam was transmitted via a telescope to a mountain top 1500m distant. The light path curved upward slightly, and beautiful color pictures were photographed at night (details omitted).

On June 4, 1988, it was sunny. The authors spent the whole day continuously observing the actual effects of turbulence on the 6.33nm laser beams. By using a receiving screen placed on a vertical wall on the mountain top, the actual variation of light spot position with time at the screen surface were recorded in

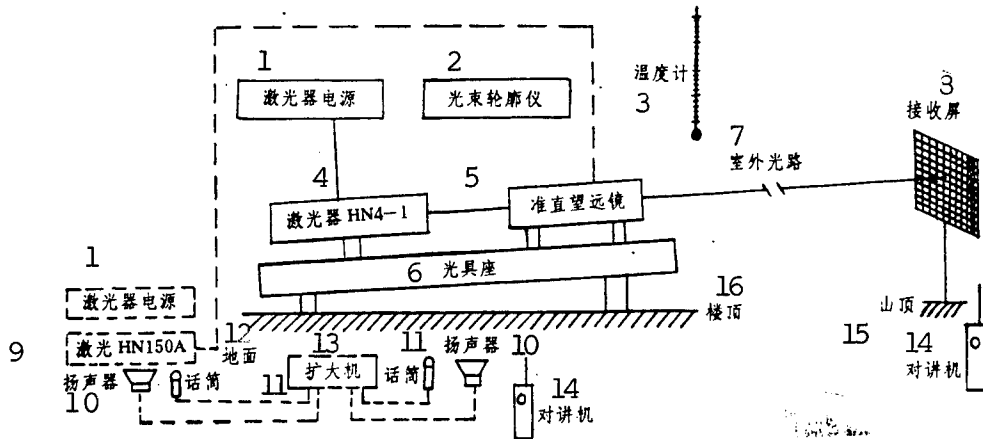


Fig. 1. Layout of observation equipment
 KEY: 1 - power supply of laser device 2 - laser beam profile instrument 3 - thermometer 4 - laser device
 5 - alignment telescope 6 - light instrument mount
 7 - outdoor light path 8 - receiving screen
 9 - laser 10 - loudspeaker 11 - telephone
 12 - ground surface 13 - audio amplifier
 14 - intercom 15 - mountain top 16 - top of building

detail. The appended table lists the original data of the on-site recording. We can see that there were very small variations of the light-spot position horizontally. Fig. 3 shows the variation of light spot center position in the direction vertical to the ground surface over time. The length of the vertical line indicates the maximum amplitude of the instantaneous deviation of light spots from the steady position. Obviously, there were interferences from multiple factors. However, the occasional interference restored to equilibrium generally in about 0.2s. From the entire curve, we can see that the positions of the light spots are the lowest in the morning and at night. If the light spot position at 7:30 in the morning was used as the origin of coordinates (0,0), then the light-spot equilibrium position after sunrise rises along the Y-axis, to arrive at the highest position (0,11) at 12:30 near midday. Then the position stays basically unchanged until past 19:15 in the afternoon, with slow descent of the light spots. At 22:30 hours, the light spots returned almost to the origin (0.3). The residual value of 3cm along the Y-direction accounts for the unique feature of summer atmospheric

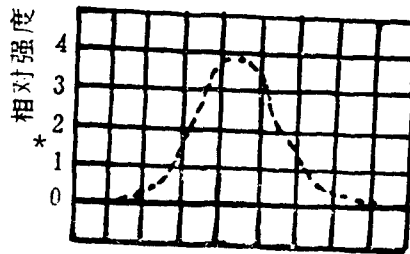


Fig. 2. Distribution of light beam intensity on a cross-sectional surface
 * = relative intensity

temperature in the Wuhan area, with very slow temperature declines at the ground surface before midnight. Generally speaking, light-spot drift is relatively larger from 10:00 hours in the morning to 18:00 hours in the afternoon, and the drift is relatively small in the night to before sunrise. Within 7:30 to 8:15 hours, the greatest drift along the curve is due to multiple factors of vibrating light source because this was the rush hour of the day when people went to work, and the building had occasional vibrations. A study of the effect of such vibrations is also one of the authors' tasks. This will be reported in a separate article.

As indicated by numerous actual observations, light-spot drift changes throughout the day, being small at night and large in the day, with the minimum at one hour before sundown and after sunrise, and the maximum several hours after midday. By reference to the appended table, if the light-spot drift values corresponding to Fig. 3 used to calculate the refractivity structure constant C_n varies with time, we can obtain a curve similar to that obtained by American researchers (Fig. 4) [4]. However, the curve plotted by the American researchers was recorded on the mountain side near Boulder, Colorado, by using pulsation thermometers. Thermometers were placed on fixed

Appended table
 COORDINATES OF LIGHT-SPOT POSITIONS EXHIBITED ON
 RECEIVING SCREENS AT MOUNTAINSIDE ON JUNE 4, 1988

| | | | | | | | | | | | | | | |
|--------------|---|--------|---------|-----------|------------|----------|---------|----------|-----------|---------|--------|----------|----------|-------|
| 时间(h:min) | 1 | 7:30 | 7:50 | 8:15 | 8:25 | 8:30 | 8:35 | 8:45 | 9:00 | 9:15 | 9:30 | 9:45 | | |
| 坐标(x, y)(cm) | 2 | (0,0) | (0,1) | (0,2) | (0,3) | (0,4) | (0,5) | (0,6) | (0,6.5) | (0,7) | (0,8) | (0,8.5) | | |
| 漂移最大值(cm) | 3 | 3.0 | 3.0 | 2.0 | 1.5 | 1.3 | 1.0 | 1.0 | 1.0 | 1.5 | 1.0 | 1.0 | | |
| 时间(h:min) | 1 | 9:52 | 10:00 | 10:35 | 11:00 | 11:30 | 12:00 | 12:30 | 13:00 | 13:30 | 14:00 | | | |
| 坐标(x, y)(cm) | 2 | (0,9) | (0,9) | (0,9) | (0,9) | (0,9.5) | (-1,10) | (0,11) | (0,10) | (0,9.5) | (0,9) | | | |
| 漂移最大值(cm) | 3 | 3.0 | 2.0 | 1.2 | 1.5 | 1.5 | 1.5 | 2.0 | 2.0 | 1.5 | 2.0 | | | |
| 时间(h:min) | 1 | 14:30 | 15:00 | 15:30 | 16:00 | 16:30 | 17:00 | 17:30 | 18:00 | 18:30 | 19:00 | 19:25 | | |
| 坐标(x, y)(cm) | 2 | (0,10) | (-1,10) | (-1.5,10) | (-1.5,9.5) | (-1.5,9) | (-1,9) | (-0.5,9) | (-0.5,10) | (0,11) | (0,11) | (0,11) | | |
| 漂移最大值(cm) | 3 | 2.0 | 2.0 | 1.5 | 2.0 | 1.5 | 1.2 | 3.0 | 2.0 | 0.4 | 0.4 | 0.4 | | |
| 时间(h:min) | 1 | 20:00 | 20:30 | 20:45 | 21:00 | 21:15 | 21:30 | 21:37 | 21:45 | 21:55 | 22:00 | 22:15 | 22:20 | 22:30 |
| 坐标(x, y)(cm) | 2 | (0,10) | (0,9) | (0,8) | (2,7) | (0,7) | (0,5) | (0,4.5) | (0,4.5) | (0,3.5) | (0,3) | (-0.5,3) | (-0.5,3) | (0,3) |
| 漂移最大值(cm) | 3 | 0.7 | 0.6 | 1.0 | 1.0 | 0.5 | 0.5 | 0.5 | 0.5 | 0.5 | 0.5 | 0.5 | 0.6 | 0.5 |

KEY: 1 - time 2 - coordinates 3 - maximum drift value

positions on the rocky mountain platforms, with ground unevenness being 0.3m. The value C_T was measured with a pulsation thermometer and C_n was calculated by using Eq. (7). Obviously, this variation in the refractivity structure constant was due to local turbulence. However, the variation in C_n calculated by the present authors by using the observed light-spot drift values, is due to the overall effect of turbulence on the entire light path.

Now we calculate the curved-upward curvature of the light path by using Eq. (8). The maximum value of $h=11\text{cm}$ is substituted as the light-spot deviation at 12:30 hours in the appended table. Since $L=1.5\text{km}$, therefore

$$C = \frac{-2h}{L^2} = \frac{-11 \times 10^{-6} \times 2}{1.5^2} = -98 \text{ (}\mu\text{rad/km)}$$
 the negative sign indicates curved upward.

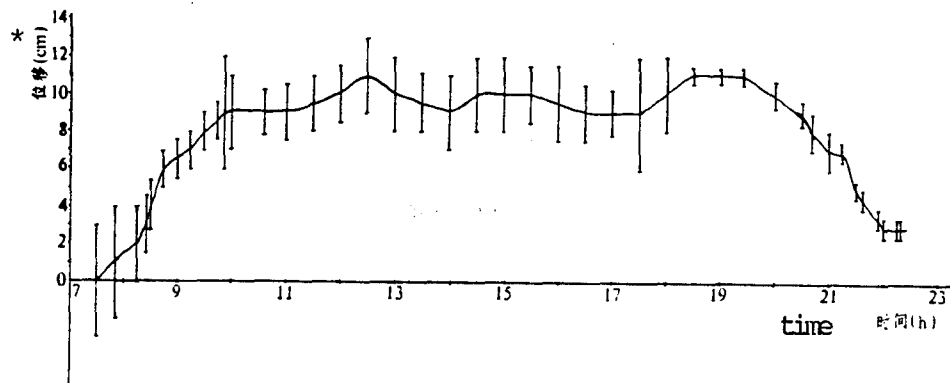


Fig. 3. Variation of light-spot position on receiving screen on June 4, 1988
* = displacement

Moreover, Eq. (9) can be used to calculate that the approximate value of the temperature gradient is

$$\frac{dT}{dh} = (-98 - 32.6) / 0.93 = -140 (\text{K/km})$$

The measured temperature gradient is approximately -100K/km . Both values are consistent in order of magnitude. Considering that the light-spot deviation of 11cm is the maximum value, the theoretical and measured values agree quite well.

Fig. 5 indicates the time variation curve of the refractivity coefficient k as measured by Soviet researchers [5]. At high noon in May, the refractivity K was 0.5 to 6.5 . Based on their definition that K is the ratio of the earth's radius to the light beam radius curvature, we can obtain the conclusion that the curvature of the light beam transmission path is

$$* = \text{earth} \quad C = \frac{K}{R_{\text{地}}^*} = \frac{0.5 \sim 0.65}{6.37 \times 10^6 \text{ m}} = (78.2 \sim 102) (\mu\text{rad/km})$$

This just includes our measured value of 98mrad/km . Therefore, we used the simplest method to obtain the results of the observation, consistent not only in the variation trend over a day with that of the American researchers, but also in the

absolute values consistent with the Soviet researchers.

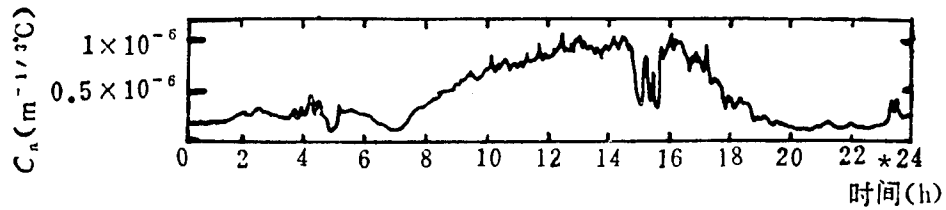


Fig. 4. Variation of refractivity structure constant measured on Colorado mountain area in the United States
KEY: * = time

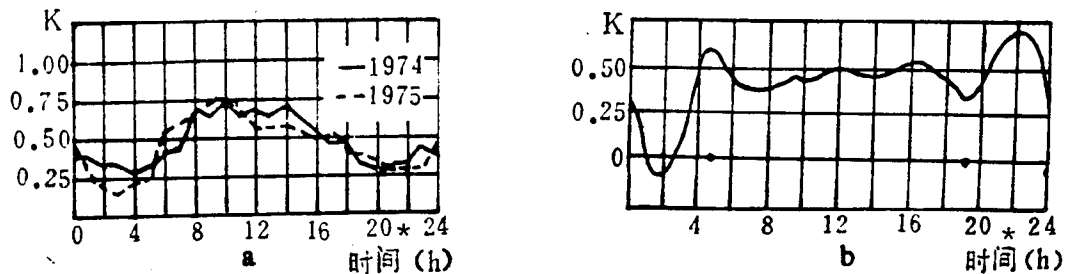


Fig. 5. Variation of refractivity coefficient induced by atmospheric turbulence measured by Soviet researchers
LEGEND: a - variation for the same month at same location, but in different years
b - variation of mean value in May at location thus determined
KEY: * - time

During the entire day of June 4, 1988, the variation of the light spots on a receiving screen placed on the mountainside is shown in Fig. 6. On the horizontal axis (the east-west direction), the light-spot center remained almost unchanged. This explains that the day was a sunny wind-free day. Fig. 7 shows the light-spot-center drift on the receiving screen on the mountain side on June 6, 1989. The dashed line indicates the

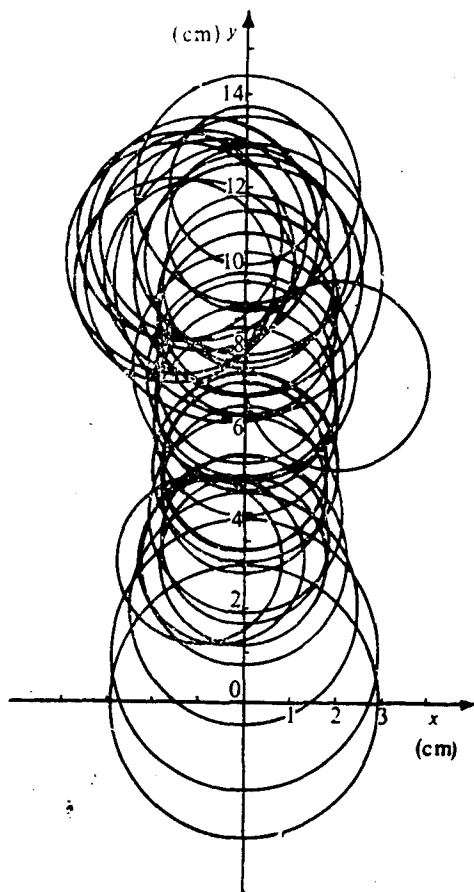


Fig. 6. Deviation and drift of light spot on June 4, 1988
 LEGEND: Circles indicate light-spot activity range at a certain time

maximum variation range of the light-spot edge over several hours. Fig. 8 shows a color picture of the light spots photographed on the mountainside during measurements, with the coordinate center $(-1.5, -2.3)$ and the dimension, about 5.5cm.

Around 20:30 hours on May 13, 1988, the observed light-spot drift was only 0.5cm. Over a long observational period from April to June, 1988, and again over a long observation period May to July, 1989, the maximum probability value of the light-spot

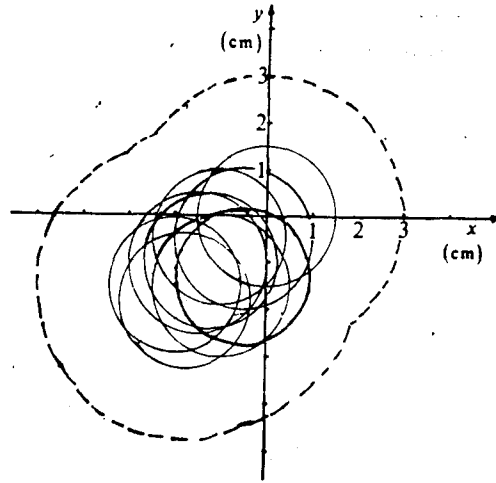


Fig. 7. Drift of light-spot center observed at a mountainside on June 6, 1989.
 LEGEND: Dashed line indicates the activity range of light spots along the edge.

drift is $2\delta=1.0\text{cm}$; the value approaches 2.0cm in a short time. Thus, we can deduce that the range of the light-beam drift angle is

$$\sigma_a = \frac{1}{2} \cdot \frac{2\delta_d}{L} = \frac{1}{2} (0.5 \sim 2.0) \times 10^{-5} / 1.5 = (1.7 \sim 6.7) \text{ } (\mu\text{rad})$$

If the median value 4.0mrad is taken, and considering that the actual pupil size of the emitting light beam $\omega_0=3.2\text{cm}$ to be substituted in Eq. (11), then we obtain

$$C_n^2 = \frac{\sigma_a^2 \omega_0^{1/3}}{1.75L} = \frac{4^2 \times 10^{-12} \times (3.2 \times 10^{-2})^{1/3}}{1.75 \times 1.5 \times 10^3} = 19.4 \times 10^{-16} (\text{m}^{-2/3})$$

This is the range of intermediate turbulence, due to quite a number of trees, flowers, and grass in the school campus below the optical path.

The light-beam expansion angle due to turbulence can be given with Eq. (12).

$$\theta = 4.03(4.4 \times 10^{-8})^{6/5} \times (0.633 \times 10^{-6})^{-1/5} \times (1.5 \times 10^3)^{3/5} = 8.4 \text{ (}\mu\text{rad)}$$

Thus, we can deduce that the light-spot dimensions on the

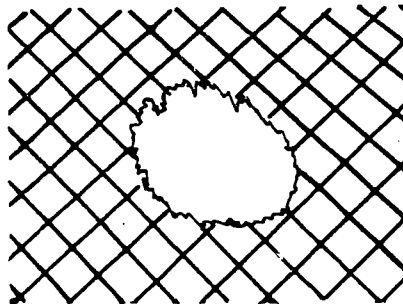


Fig. 8. Coordinates (-1.5, -2.3) of light-spot center, $\phi = 5.5\text{cm}$ in a picture photographed from an observation screen

receiving screen is
[four lines]

$$\theta \cdot L = 8.4 \times 10^{-6} \times 1.5 \times 10^3 = 12.6 \text{ (cm)}$$

This is 100% greater than the actual measured value. If the smaller value 2.0mrad is selected from the range (1.7 to 6.7)mrad, for the calculated drift angle, the value corresponds to 1.0cm, the drift value of most light spots, then the calculated $C_n = 2.2 \times 10^{-6} \text{m}^{-1/3}$ is still in the intermediate-turbulence range, but on the small side. Here, we can calculate that the light-spot dimension is 5.5cm, which is just consistent with the measured value (Fig. 8). However, on the night of June 1989, with level 3 to level 4 wind blowing, the light spots' picture we obtained on the receiving screen with dimensions about 12.6cm (Fig. 9), which is on the larger side of intensity for the

intermediate turbulence $C_n=4.4 \times 10^{-8}$ ($m=1/3$).

Eq. (10) can be used to estimate the observational results of light spot scintillation; this is not serious in most kinds of weather. With respect to a converging light beam, we have

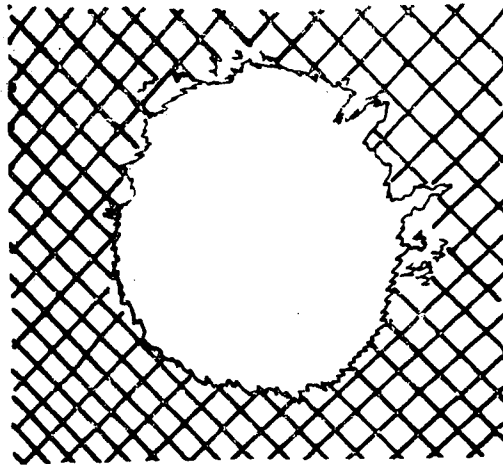


Fig. 9. Scattering of light spots due to intermediate turbulence ($\phi=12.6\text{cm}$)

$$\sigma_I^2 = 0.31(2\pi/0.633)^{7/6} \times 10^7 \times (1.5 \times 10^3)^{11/6} \times (2.2 \times 10^{-8})^2 = 0.014$$

From the variance of logarithmic intensity σ_I^2 , we can estimate that mostly the value of I_0/I is 1.13. If $C_n=4.4 \times 10^{-8} \text{m}^{-1/3}$ is substituted into the above equation, then the light-intensity fluctuation is 1.25, exhibiting relatively weak scintillation. This is consistent with most night observations on the mountainside. However, on the night of April 22, 1988, the authors observed a much different situation on the light path 0.85m over a flat cement road. Since the transmission distance was 1.65m, and the light-beam divergence angle was 1.4mrad, there was no clear boundary of light spots on the receiving screen,

with dimensions approximately 24cm. In the continuous observation from 20:00 to 22:00 hours at night, no deviations or drift of the light spot were detected, but with intensive scintillation. The light spots were affected by quite a number of vortices. These vortices induced independent scattering and diffraction on the laser beam passing through them, and also



Fig. 10. Effect on TEM₀₀ mode light beam due to intensive turbulence

formed random interferences on the receiving screen. The daytime temperature was relatively high (290K), and rains had fallen several days ago. Therefore, the cement road with sufficient moisture absorbed, after a temperature rise during the day, the temperature was difficult to reduce at dusk. People walking on the road could feel hot air rising upward. This intensive turbulence phenomenon could not quickly abate because of the lack of wind; therefore, it induced great fluctuation in intensity in the large-dimensional region of the light spots. We could observe random variations quite sharply between the dark region and the bright region as shown in Fig. 10. If $I_0/I=2$ is substituted in Eq. (10), then the estimate refractivity structure constant is

$$C_n = \frac{\ln 2}{\sqrt{0.49}} \left(\frac{2\pi}{\lambda} \right)^{-\frac{7}{12}} L^{-\frac{11}{12}} = 0.99 \left(0.623 \times 10^6 \right)^{-\frac{7}{12}} (167)^{-\frac{11}{12}} = 7.5 \times 10^{-7} (\text{m}^{-\frac{1}{3}})$$

that is, of a very intensive turbulence range.

Preliminary Conclusions

A laser beam emitted from the top of a tall building, to pass through over the campus of the Huazhong University of Science and Engineering at a height of little more than 50m, transmitted toward the mountain top or mountainside of Yujia Mountain, beside the East Lake. The effect of atmospheric turbulence was much smaller than the near-ground transmission of the laser beam. Even in the summer month of July, under ordinary weather conditions, turbulence along this light path was in the range between weak to intermediate turbulence. The reason is related to the natural environment, in which quite a number of trees, flowers, and grass were beneath this light path. These evergreen plantings adjust the temperature gradient along the light path not to vary intensively and randomly; therefore, this is an ideal site to study the interaction between the atmosphere and laser beams, especially intense laser beams, in the transmission process. This has important practical value, whether in civilian or military applications. This provides a good basis for studying the atmospheric transmission of lasers by a key laser technology laboratory, which is open to the public.

Jiang Hongbin, Zhang Yixian, Peng Wenyan, and Chang Xiaocheng, students in the graduating class in the laser specialty, department of optics, Huazhong University of Science and Engineering, took part in some of the experimental work.

The article was received for publication on October 28, 1991.

DISTRIBUTION LIST

DISTRIBUTION DIRECT TO RECIPIENT

| <u>ORGANIZATION</u> | <u>MICROFICHE</u> |
|----------------------------------|-------------------|
| B085 DIA/RTS-2FI | 1 |
| C509 BALLOC509 BALLISTIC RES LAB | 1 |
| C510 R&T LABS/AVEADCOM | 1 |
| C513 ARRADCOM | 1 |
| C535 AVRADCOM/TSARCOM | 1 |
| C539 TRASANA | 1 |
| Q592 FSTIC | 4 |
| Q619 MSIC REDSTONE | 1 |
| Q008 NTIC | 1 |
| Q043 AFMIC-IS | 1 |
| E404 AEDC/DOF | 1 |
| E410 AFDTC/IN | 1 |
| E429 SD/IND | 1 |
| P005 DOE/ISA/DDI | 1 |
| 1051 AFIT/LDE | 1 |
| PO90 NSA/CDB | 1 |

Microfiche Nbr: FTD96C000235
NAIC-ID(RS)T-0697-95